

LETTER

Enhanced light extraction efficiency of micropixel geometry AlGaN DUV light-emitting diodes

To cite this article: Richard Floyd et al 2021 Appl. Phys. Express 14 084002

View the <u>article online</u> for updates and enhancements.

LETTER

Enhanced light extraction efficiency of micropixel geometry AlGaN DUV light-emitting diodes



Richard Floyd * D, Mikhail Gaevski, Kamal Hussain, Abdullah Mamun, MVS Chandrashekhar, Grigory Simin, and Asif Khan

Department of Electrical Engineering, University of South Carolina, Columbia, SC 29208, United States of America

*E-mail: rsfloyd@email.sc.edu

Received May 27, 2021; revised June 22, 2021; accepted June 29, 2021; published online July 15, 2021

We report a 1.8 times improved light extraction efficiency for truncated cone AlGaN DUV (275 nm emission) micropixel LEDs when the pixel size was reduced from 90 to 5 μ m. This is a direct consequence of reducing the re-absorption of sideways-travelling photons, as the lateral absorption length was measured to be 15 μ m using cathodoluminescence. We also investigated the effect of an Al₂O₃/Al sidewall coating on the device performance which led to an on-wafer pulsed-mode brightness of 10.3 kW cm⁻² from a single 5 μ m truncated cone micropixel. © 2021 The Japan Society of Applied Physics

II-nitride materials-based visible emission LEDs have emerged as a disruptive technology in the fields of lighting, 1) communications, 2-4) and displays. 5,6) Shorter wavelength LEDs in the DUV spectral region (210 nm-360 nm) with ultra-wide bandgap (UWBG) Al_xGa_{1-x}N active layers are now poised to displace toxic Mercury-based light sources.⁷⁾ Over the past decade AlGaN LEDs operating in the DUV spectral region ($\lambda_{\text{emission}} < 300 \text{ nm}$) have been deployed in novel applications including autonomous drone-based sterilization and sanitization systems, ⁸⁾ point-of-use water purification systems, ⁹⁾ photo-therapeutics, ¹⁰⁾ gas sensors, ¹¹⁾ and nonline-of-sight (NLOS) communications. 12) Nevertheless, the external quantum efficiency (EQE) of AlGaN materials-based DUV LEDs is still significantly lower than that of their visible counterparts. 10) The low EQE is primarily due to the low light extraction efficiency (LEE) and the device thermal management issues. 13,14) Unlike visible LEDs, the strong absorption of DUV photons by the p-GaN hole-supply layer and traditional Ni/Au contact metal stack leads to a near complete loss of the upwards-travelling TE-polarized photons. Thus, extraction of the emitted radiation is best accomplished using flip-chip LEDs through the substrate-side of the wafer. However, the widespread use of low-cost, non-conductive sapphire substrates restricts the extraction cone to $\pm /-22^{\circ}$, significantly lowering the substrate-side LEE. 15) Furthermore, the transverse magnetic/ transverse electric (TM/TE) polarization ratio increases with active region Al-content, leading to an increased number of inplane photons which are quickly re-absorbed. 16,17) To avoid excessive absorption of the Al_xGa_{1-x}N active region emission travelling toward the substrate, an even higher Al-content transparent n-contact Al_xGa_{1-x}N epilayer is required. Since the ionization of the p- and n-dopant acceptors and donors decreases with increasing Al mole-fraction, such high-Al ncontact layers can potentially lead to significant currentcrowding and series resistance/thermal issues. 18)

Previously, our group has shown that compared to traditional geometry large-area LEDs, interconnected DUV micropixel LEDs (micro-LEDs) can reduce the device series resistance, largely alleviating the current-crowding, thereby improving reliability, and increasing the maximum light output power (LOP) via a reduction of the thermal resistance. We also demonstrated a high-density dot-matrix 280 nm emission micro-LED display with a pixel size of $\sim\!\!25\,\mu\text{m},^{22)}$ with independent control of the pixels, a requirement for applications such as direct-write lithography.

Formation of Fresnel micro-lenses directly on the sapphireside of micro-LED wafers for their integration in optical systems was also reported.²³⁾ Recently, micro-size DUV emitters were surveyed for use in optical wireless communications (OWC) and data-transfer links. 24) To-date, the highest reported modulation bandwidth for a DUV LED is 570 MHz and was enabled by a single $20 \,\mu m$ diameter AlGaN micro-LED with a peak LOP of 130 μ W.²⁵⁾ Despite the reduced emission area for AlGaN-based micro-LEDs, the brightness (W cm⁻²) is remarkably enhanced due to their efficient light generation at kA cm⁻²-level current densities enabled by a superior removal of the self-generated heat from the device active region.²¹⁾ At these levels of injection current density, the dynamic carrier lifetimes which chiefly dictate the maximum modulation bandwidth for micro-LEDs is also significantly reduced. 26,27) Hence, increasing the LEE and the peak brightness for DUV micro-LEDs is of particular benefit for high-bandwidth optical systems.

One powerful technique to increase the LEE of DUV LEDs is by slanting the mesa sidewalls to efficiently redirect the in-plane TM-polarized photons toward the substrate for extraction. 28) Since the first report of this truncated cone architecture for DUV devices, there have been several studies on the effect of the sidewall angle and the sidewall reflector on the device performance. 29-31) However, no studies of the device size dependence of the LEE for truncated cone DUV LEDs have been reported. In this letter, we present such a study for slanted sidewall devices with pixel sizes ranging from 5–15 μ m (as defined by the p-contact diameter). In addition, standard 90 μm macro-pixel devices were fabricated on the same wafer. We also explore the effect on the device LEE and the maximum LOP from using a semi-reflective Al₂O₃/Al sidewall coating which reduces the sidewall reflectivity but improves the heat spreading. For this study, devices with both vertical and slanted sidewalls were fabricated on the same 2" wafer and they had well-matched current-voltage (I-V) characteristics.

Similar to our previous report, 21 the epi-structure for our devices consists of a double-side polished sapphire substrate, a low defect density 3 μ m thick AlN buffer layer, 32 a 3.0 μ m thick n⁺-Al_{0.65}Ga_{0.35}N n-contact layer followed by a 4-pair AlGaN-based MQW active region, a 20 nm p-Al_{0.8}Ga_{0.2}N electron block layer, a 55 nm polarization-doped reverse

graded p-Al_xGa_{1-x}N ($x = 0.7 \rightarrow 0.0$) layer, and a 250 nm p⁺-GaN hole-supply cap layer.

For the devices with slanted sidewalls, the mesa photoresist (PR) pillars were first shaped into hemispherical domes by exposing the developed PR pattern to UVA irradiation, which lowers the melting point and improves the temperature stability of the mask. This was followed by time dependent thermal-reflow (TDTR) to form hemispherical domes. Then, mesa etching was performed for both slanted and vertical sidewall devices using a Cl₂/Ar chemistry by inductively coupled plasma reactive ion etching (ICP-RIE). The diameters of the top of the mesa pillars were respectively 94, 20, 15, and 9 μ m for the 90, 15, 10, and 5 μ m pixel sizes. Further details of the fabrication procedure are elsewhere.²¹⁾ The scanning electron micrograph (SEM) of Fig. 1 shows a representative slanted sidewall profile and highly conformal coverage of the Al₂O₃/Al sidewall coating, for a 5 μ m pixel, after the device fabrication is complete. The sidewall angles were 25°, 45°, 48°, and 48° for the 90, 15, 10, and 5 μ m pixels, respectively. Varying the sidewall angle from 28°–40° was reported to have a small effect (< 0.1%) on the overall device EQE.²⁹⁾ Hence, changes in the LEE from this angular difference are expected not to significantly alter the results of this study. The specific contact and sheet resistances were $1.64 \times 10^{-4}~\Omega \cdot cm^2$ and $80~\Omega/\Box$ for the n-side and $3.86 \times 10^{-4}~\Omega \cdot cm^2$, $91~k\Omega/\Box$ for the p-side.

We first measured the lateral absorption length for the DUV emission of our devices. For the measurement, a JEOL SEM with an UV-enhanced GATAN MonoCL-2 cathodoluminescence (CL) system and a DigiScan beam control unit was used to perform a CL line-scan across the mesa of a 90 μ m uncoated pixel with a slanted sidewall profile (see Fig. 2). An accelerating voltage of 10 keV was chosen to maximize the CL light emission from the MQW, located at a depth of \sim 0.4 μ m. This approach is like that used for determining the lateral absorption length of an AlGaN laser diode structure. The monochromatic ($\lambda_{\rm detection} \sim 275\,{\rm nm}$) CL signal, which is comprised of an exponentially varying TM-polarized component riding on top of a constant TE-polarized component, was smoothed with a 10-point average, and then fitted with an exponential curve to extract the in-plane absorption coefficient

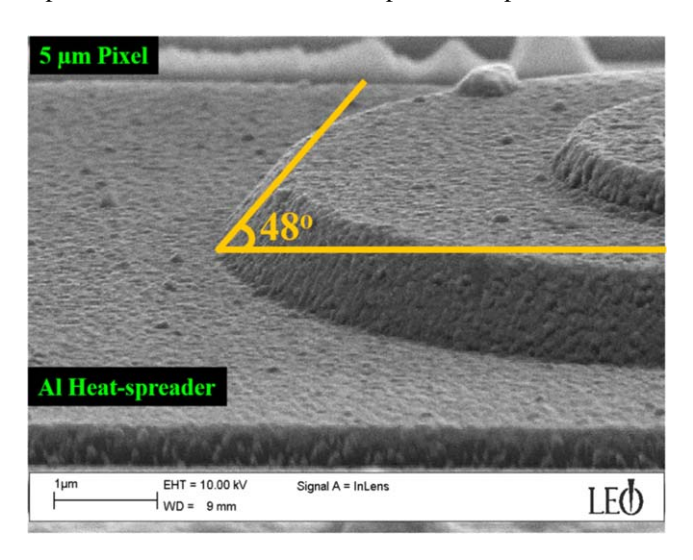


Fig. 1. (Color online) SEM imaging of the sidewall profile for a 5 μ m truncated cone micropixel showing the conformal coverage of the Al₂O₃/Al heat-spreader and the sidewall profile.

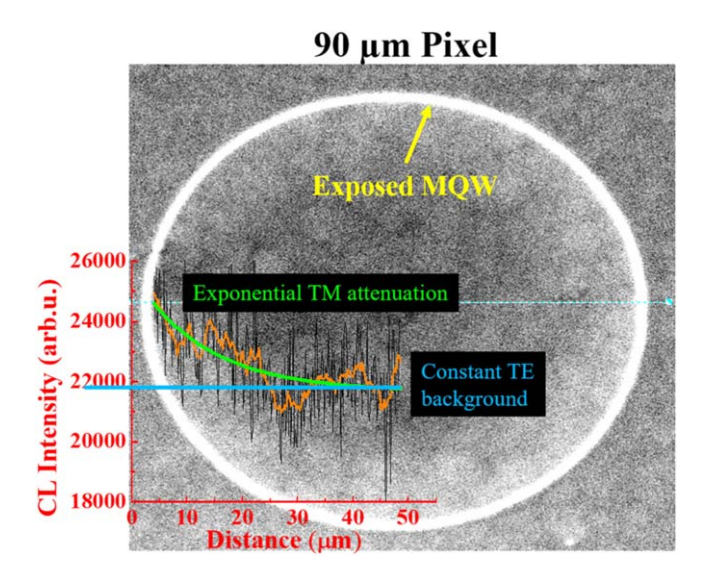


Fig. 2. (Color online) Cathodoluminescence imaging of a truncated cone $90~\mu m$ micropixel before contact metallization with the monochromatic intensity plot overlaid. The CL signal was smoothed by a 10-point average and then fitted with an exponential curve to extract the lateral absorption length for our device epi-structures. The signal from the exposed MQW region was not included in the absorption length extraction.

(α). By mapping the CL line-scan intensity to the SEM-measured mesa diameter, the lateral absorption length within the mesa structure was estimated to be $\sim 15 \, \mu \mathrm{m}$ ($\alpha = 667 \, \mathrm{cm}^{-1}$), which is similar to the previously established value of $10 \, \mu \mathrm{m}$ ($\alpha = 1000 \, \mathrm{cm}^{-1}$) for the MQW active region of DUV LEDs determined by the Monte Carlo simulation. ^{13,34}) Hence, considering the measured lateral absorption length of only $15 \, \mu \mathrm{m}$, keeping the lateral travel distance for DUV photons to sub-20 $\mu \mathrm{m}$ is critical for improving the LEE and the EQE of UWBG AlGaN MQW LEDs.

To validate this assertion and study the size-dependent effects, current-voltage-output power (I-V-L) and EQE measurements were made on individual micropixels with bare sidewalls (after p-metallization). Measurements were repeated after the devices were blanketed with a semi-reflective Al₂O₃/Al heat-spreader to study of the trade-off between the increased heat spreading for the devices which improves light generation for micro-LEDs,²¹⁾ and the reduction of sidewall reflectivity.³⁰⁾ All measurements were made on-wafer using a calibrated photometer and a photodiode. The electroluminescence (EL) emission spectrum was collected using a fibercoupled Horiba monochromator with a LN₂-cooled CCD array.

Figure 3 shows the I-V-L curves (inset shows the EL spectra) for the vertical and slanted sidewall micro-LEDs under DC current injection, demonstrating increased LOP and well-matched electrical characteristics for micropixels of the same size. Figure 4 shows the DC I-V-L characteristics of the devices after the deposition of a semi-reflective Al_2O_3/Al heat-spreader. The I–V characteristics of the devices were unchanged after the sidewall coating; although, the maximum LOP increased for all the devices compared to the bare sidewall condition. Interestingly, the onset of LOP saturation is also much softer for the sub-20 μ m micropixels with slanted sidewalls compared to those with vertical sidewalls, indicating superior thermal management. This, we believe, arises from the highly conformal sidewall coverage of the

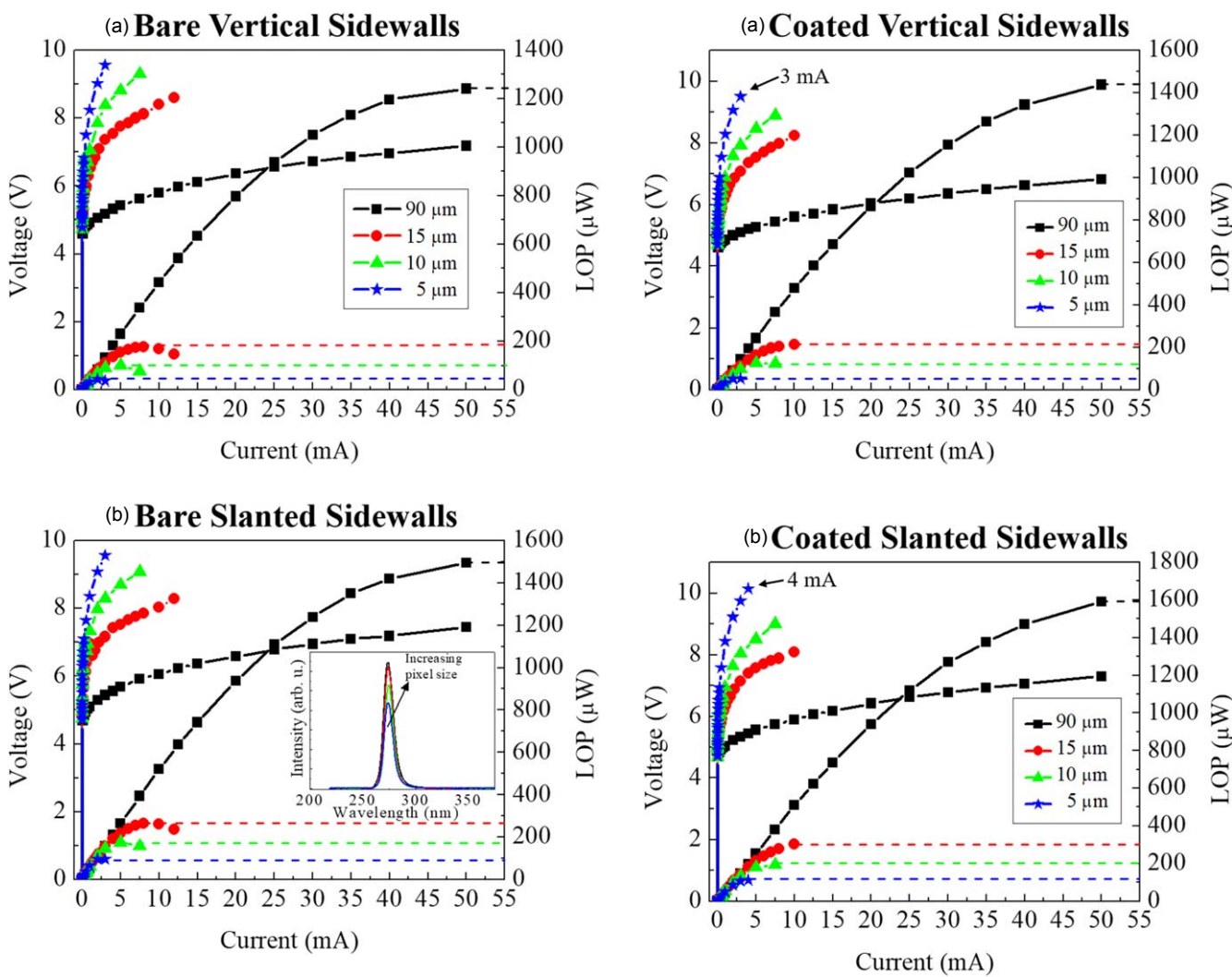


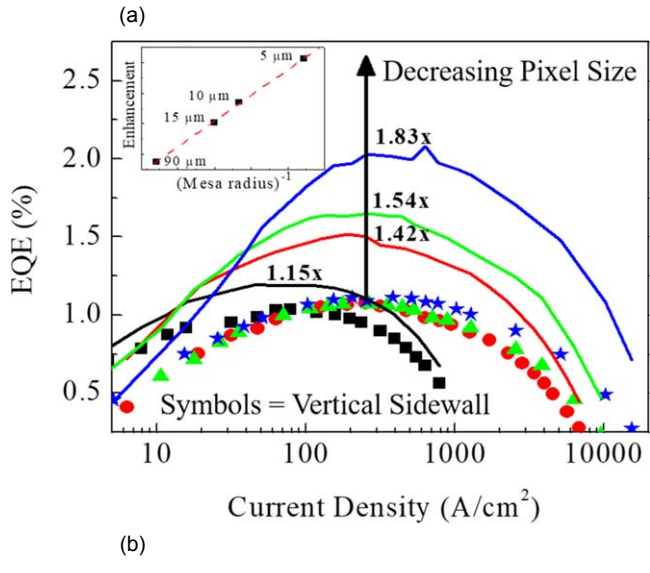
Fig. 3. (Color online) DC-drive I-V-L characteristics for bare-sidewall devices with (a) vertical sidewalls and (b) slanted sidewalls. The legend of (a) applies to both plots and the inset of (b) shows the representative electroluminescence emission spectra for the devices of this study. The peak EL emission is 275 nm.

Fig. 4. (Color online) DC-pump I-V-L characteristics for devices equipped with the semi-reflective Al₂O₃/Al heat-spreader having (a) vertical sidewalls and (b) slanted sidewalls.

blanket Al_2O_3/Al heat-spreader in the case of the slanted sidewall devices, providing a larger surface-area for transferring the self-generated heat out of the mesa pillar, as opposed to our vertical-walled devices where the heat-spreader only contacts the metallized p-electrode.²¹⁾

In Fig. 5(a), we present the EQE of the vertical and slanted sidewall devices, before the Al₂O₃/Al coating, which shows a strong pixel size-dependent enhancement for the slanted sidewall devices. Because the EQE is the same for all the vertical-walled devices, we preclude the possibility of sizedependent current injection efficiency (CIE) or internal quantum efficiency (IQE) improvements as the primary drivers of the EQE enhancement for the identically sized slanted sidewall devices. Therefore, the size dependent EQE enhancement is wholly attributed to an improvement of the device LEE. In direct agreement with the result of the CLmeasurement, this LEE enhancement strongly depends on the lateral travel length for in-plane DUV emission resulting in a near exact inverse dependence on the mesa radius "r" [see inset to Fig. 5(a)]. It is well-established in DUV LEDs that TM-polarized emission propagates in-plane (laterally) from the point of generation whereas TE-polarized emission travels mostly in the vertical direction. $^{13,16,28)}$ This implies that the marked LEE enhancement is predominantly from an increase in the out-coupling of TM-polarized photons. Hence, for traditional geometry broad-area devices, only the in-plane (TM-polarized) emission which is generated within a few absorption lengths of the mesa perimeter can be extracted. This is exacerbated as $\lambda_{\rm emission}$ is shortened and the TE/TM emission ratio decreases. Thus, the micro-LED platform and truncated cone architecture provides an attractive route for improving the LEE as the MQW Al-content is increased.

In Fig. 5(b) we compare the EQEs for the slanted sidewall devices before and after the Al₂O₃/Al coating. In the case of the devices with the sidewall-coating, the thermal droop lessened, the rising-edge slope of the EQE shallowed, and the peak EQE position shifted to a higher current density, indicating improved thermal management at the expense of LEE. This thermal benefit is the primary driver of the improved EQE at high injection current density, evidenced by the cross-over points in Fig. 5(b); it is responsible for the enhanced peak LOPs observed in Fig. 4. However, the size-dependent decrease of the peak EQE after the addition of the Al₂O₃/Al heat-spreader indicates a significant reduction of the sidewall reflectivity. It has been suggested that one may



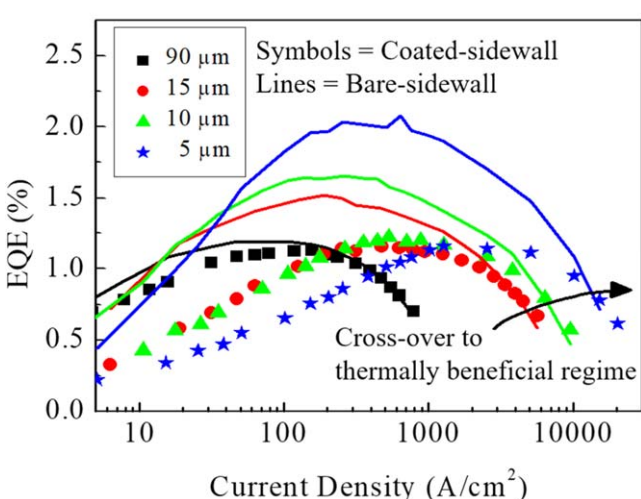


Fig. 5. (Color online) Comparison of the EQE for (a) the vertical and slanted sidewall devices with bare-sidewalls to determine the size-dependent LEE enhancement and (b) the slanted sidewall devices before and after the Al₂O₃/Al sidewall coating elucidating the improved thermal management at the expense of LEE. The inset to (a) shows the strong (1/r) dependence of the LEE enhancement factor on the mesa radius (r) and the legend of (b) applies to both plots.

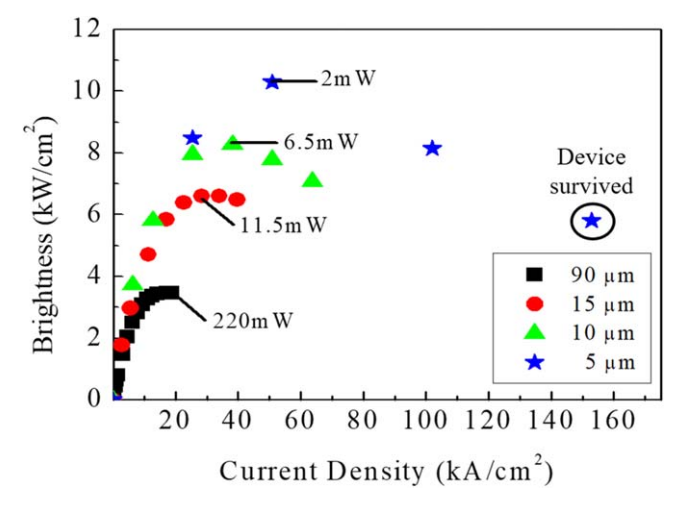


Fig. 6. (Color online) Pulsed-mode I-L characteristics for slanted-sidewall devices equipped with the semi-reflective Al_2O_3/Al heat-spreader. The duty cycle was 0.05% and the pulse-width was 500 ns.

expect such reduction arising from the roughness induced optical losses of the conformal metallic sidewall reflector.³⁰⁾ In that report, the authors demonstrated that it can be largely circumvented for interconnected micropixel arrays by using a narrow grid-geometry interconnect, although the thermal consequences were not studied. In this work, the reduced sidewall reflectivity caused by the Al₂O₃/Al heat-spreader was eventually overcome by the marked improvement of the device thermal management. Highlighting the overarching criticality of minimizing selfheating effects and the lateral travel length of DUV photons for AlGaN LEDs. The 5 μ m pixel devices reported here had a record brightness of 570 W cm⁻² at a DC-drive current of 4 mA when equipped with the heat-spreader and the highest LEE enhancement factor of 1.83-fold before the sidewallcoating.

As an exemplary demonstration of the potential of sub-20 μ m AlGaN DUV micro-LEDs, we also tested our heat-spreader equipped slanted sidewall micropixels in the pulsed-mode to reduce the self-heating effect from on-wafer measurements. The testing was conducted using a 500 ns pulse-width and 0.05% duty-cycle (Fig. 6). Under these conditions, the kW cm⁻²-class emission brightness of our devices surpasses that of DC-biased highly emissive visible micro-LEDs by at least one order of magnitude, $^{35-37}$) a potentially revolutionary advance arising from the robustness of deeply scaled AlGaN micro-LEDs and their capability to sustain extreme current densities. We believe this level of performance can be attained in DC-operation for flip-chip packaged devices with an improved sidewall reflectivity.

In summary, we studied the size-dependent LEE enhancement for truncated cone AlGaN micropixel DUV LEDs with pixel sizes of 5, 10, 15 and 90 μ m by a comparison with emission from vertical sidewall devices of identical dimensions fabricated from the same wafer. From CL measurements, the lateral absorption length of $\sim 15 \,\mu \mathrm{m}$ of our mesa structures was determined. Re-absorption of sideways travelling TM-polarized DUV photons by the MQW and p-GaN epitaxial layers is identified as one of the key factors limiting the LEE of DUV LEDs. In direct agreement with the CL measurement, from I-V-L testing we found the LEE enhancement to closely follow a 1/r dependence on the mesa radius. Hence, for DUV emitters, scaling down to device dimensions less than the lateral absorption length is critical for maximizing LEE. The peak LOP improved further after the devices were coated with a semi-reflective Al₂O₃/Al heatspreader despite the reduced LEE owed to a reduction in the sidewall reflectivity. The on-wafer measured LOP and brightness of a single 5 μ m pixel reached record levels of 2 mW (10.3 kW cm⁻²) at 10 mA (50.1 kA cm⁻²) using 500 ns pulsed-current injection at 0.05% duty-cycle. Thus, the AlGaN micropixel technology can potentially revolutionize optical communication and lighting systems operating in

This research was supported by ARO contract W911NF-18-1-0029 monitored by Dr. M. Gerhold. The characterization was partially supported the National Science Foundation (NSF), ECCS Award Nos. 1711322, 1810116, and 1831954.

ORCID iDs Richard Floyd (i) https://orcid.org/0000-0002-1073-9277

- 1) S. Nakamura, T. Mukai, and M. Senoh, Appl. Phys. Lett. **64**, 1687 (1994).
- 2) R. X. Ferreira et al., IEEE Phot. Techn. Lett. 28, 2023 (2016).
- P. Tian, X. Liu, S. Yi, Y. Huang, S. Zhang, X. Zhou, L. Hu, L. Zheng, and R. Liu, Opt. Expr. 25, 1193 (2017).
- 4) M. D. Dawson, J. Herrnsdorf, E. Xie, E. Gu, J. McKendry, A. D. Griffiths, and M. J. Strain, Imaging 10, 40 (2015).
- 5) Z. Chen, S. Yan, and C. Danesh, J. Phys. D: Appl. Phys. 54, 123001 (2020).
- 6) J. Y. Lin and H. X. Jiang, Appl. Phys. Lett. 116, 100502 (2020).
- S. Nagai, K. Yamada, A. Hirano, M. Ippommatsu, M. Ito, N. Morishima, K. Aosaki, Y. Honda, H. Amano, and I. Akasaki, J. Journ. Appl. Phys. 55, 082101 (2016).
- 8) V. Kramar, IEEE Proc. 27th Conf. Open Innovations Association (FRUCT), 2020, p. 90.
- G. Y. Lui, D. Roser, R. Corkish, N. J. Ashbolt, and R. Stuetz, Sci. Tot. Env. 553, 626 (2016).
- 10) M. Kneissl, T. Y. Seong, J. Han, and H. Amano, Nat. Photonics 13, 233 (2019)
- 11) S. Khan, D. Newport, and S. Le Calvé, Sensors 19, 5210 (2019).
- 12) Z. Xu and B. M. Sadler, IEEE Comms. Mag. 46, 67 (2008).
- 13) H. Y. Ryu, I. G. Choi, H. S. Choi, and J. I. Shim, Appl. Phys. Expr. 6, 062101 (2013).
- 14) W. Liu and A. A. Balandin, J. Appl. Phys. 97, 073710 (2005).
- 15) M. R. Krames, O. B. Shchekin, R. Mueller-Mach, G. O. Mueller, L. Zhou, G. Harbers, and M. G. Craford, J. Disp. Technol. 3, 160 (2007).
- 16) J. W. Lee, D. Y. Kim, J. H. Park, E. F. Schubert, J. Kim, J. Lee, Y. I. Kim, Y. Park, and J. K. Kim, Sci Rep. 6, 1 (2016).
- R. Floyd, K. Hussain, A. Mamun, M. Gaevski, G. Simin,
 M. V. S. Chandrashekhar, and A. Khan, Appl. Phys. Expr. 13, 022003 (2020).
- 18) M. Shatalov et al., J. Journ. Appl. Phys. 41, 5083 (2002).
- 19) V. Adivarahan, S. Wu, W. H. Sun, V. Mandavilli, M. S. Shatalov, G. Simin, J. W. Yang, H. P. Maruska, and M. A. Khan, Appl. Phys. Lett. 85, 1838 (2004).
- 20) M. Shatalov, Z. Gong, M. Gaevski, S. Wu, W. Sun, V. Adivarahan, and M. A. Khan, Int. Soc. Opt. Phot. 6134, 61340P (2006).

- 21) R. Floyd, M. Gaevski, M. D. Alam, S. Islam, K. Hussain, A. Mamun, S. Mollah, G. Simin, M. V. S. Chandrashekhar, and A. Khan, Appl. Phys. Expr. 14, 014002 (2020).
- 22) S. Wu, S. Chhajed, L. Yan, W. Sun, M. Shatalov, V. Adivarahan, and M. A. Khan, Jpn. J. Appl. Phys. 45, L352 (2006).
- 23) M. E. Gaevski, M. Shatalov, S. Wu, and M. A. Khan, MRS Proc. Lib. 916, 9 (2006).
- 24) X. He, E. Xie, M. S. Islim, A. A. Purwita, J. J. McKendry, E. Gu, H. Haas, and M. D. Dawson, Phot. Res. 7, B41 (2019).
- 25) D. M. Maclure, J. J. D. McKendry, J. Herrnsdorf, X. He, E. Xie, E. Gu, and M. D. Dawson, 2020 IEEE Phot. Conf. (IPC), 2020, p. 1.
- 26) J. J. McKendry, D. Massoubre, S. Zhang, B. R. Rae, R. P. Green, E. Gu, R. K. Henderson, A. E. Kelly, and M. D. Dawson, J. Light. Tech. 30, 61 (2011).
- A. Rashidi, M. Monavarian, A. Aragon, A. Rishinaramangalam, and
 D. Feezell, IEEE Elec. Dev. Lett. 39, 520 (2018).
- 28) J. W. Lee, J. H. Park, D. Y. Kim, E. F. Schubert, J. Kim, J. Lee, Y. L. Kim, Y. Park, and J. K. Kim, ACS Phot. 3, 2030 (2016).
- 29) Q. Chen, H. Zhang, J. Dai, S. Zhang, S. Wang, J. He, R. Liang, Z. H. Zhang, and C. Chen, IEEE Phot. Journ. 10, 1 (2018).
- J. Zhang, L. Chang, Y. Zheng, C. Chu, K. Tian, C. Fan, Y. Zhang, and Z. H. Zhang, Opt. Expr. 28, 17035 (2020).
- Y. Zheng, J. Zhang, L. Chang, C. Chu, K. Tian, Q. Zheng, Q. Li, Y. Zhang,
 W. Bi, and Z. H. Zhang, J. Appl. Phys. 128, 093106 (2020).
- S. Muhtadi, S. Hwang, A. Coleman, F. Asif, A. Lunev,
 M. V. S. Chandrashekhar, and A. Khan, Appl. Phys. Lett. 110, 171104 (2017).
- 33) Z. Zhang, M. Kushimoto, T. Sakai, N. Sugiyama, L. J. Schowalter, C. Sasaoka, and H. Amano, J. Journ. Appl. Phys. 59, 094001 (2020).
- 34) Z. Liu, K. Wang, X. Luo, and S. Liu, Opt. Expr. 18, 9398 (2010).
- 35) J. Herrnsdorf et al., IEEE Trans. Elec. Dev. 62, 1918 (2015).
- **36)** F. Templier, J. Soc. Inform. Disp. **24**, 669 (2016).
- 37) L. Dupré, M. Marra, V. Verney, B. Aventurier, F. Henry, F. Olivier, S. Tirano, A. Daami, and F. Templier, Gall. Nitr. Mats. Dev. XII. 10104, 1010422 (2017).